CHINESE OPTICS LETTERS

Vol. 21, No. 3 | March 2023

All-fiber telecom band energy-time entangled biphoton source

Yuting Liu (刘妤婷)[1,2], Junjie Xing (邢俊杰)[1,2], Zhiguang Xia (夏志广)[1,2], Run'ai Quan (权润爱)[1], Huibo Hong (洪辉博)[1,2], Tao Liu (刘 涛)[1,2], Shougang Zhang (张首刚)[1,2], Xiao Xiang (项 晓)[1*], and Ruifang Dong (董瑞芳)[1,2**]

[1] Key Laboratory of Time and Frequency Primary Standards, National Time Service Center, Chinese Academy of Sciences, Xi'an 710600, China

[2] School of Astronomy and Space Science, University of Chinese Academy of Sciences, Beijing 100049, China

*Corresponding author: xiangxiao@ntsc.ac.cn

**Corresponding author: dongruifang@ntsc.ac.cn

Received August 31, 2022 | Accepted November 11, 2022 | Posted Online March 14, 2023

We report an all-fiber telecom-band energy-time entangled biphoton source with all physical elements integrated into a compact cabinet. At a pump power of 800 μW, the photon pairs generation rate reaches 6.9 MHz with the coincidence-to-accidental ratio (CAR) better than 1150. The long-term stability of the biphoton source is characterized by measuring the Hong–Ou–Mandel interference visibility and CAR within a continuous operation period of more than 10 h. Benefiting from the advantages of compact size, light weight, and high stability, this device provides a convenient resource for various field turnkey quantum communication and metrology applications.

Keywords: energy–time entanglement; all-fiber biphoton source; Hong–Ou–Mandel interference.

DOI: 10.3788/COL202321.032701

1. Introduction

Entangled photon pairs are not only a crucial element of quantum networks[1], but also essential resources for quantum information processing systems. As the most common method of generating entangled photon pairs, the spontaneous parametric downconversion (SPDC) process can provide entanglements in diversified degrees of freedom. Among them, energy–time entanglement has attracted growing attention due to its strong temporal correlation and robustness to loss and decoherence when propagating through long-distance fiber links[2]. Till now, it has been applied in numerous fiber-based quantum communication and metrology experiments including quantum clock synchronization (QCS)[3–9], quantum key distribution (QKD)[10–13], quantum nonlocality tests[14,15], quantum microwave photonics[16], etc. However, most of the experiments were implemented over fiber spools, implying that the above research is still at the demonstration stage. For realistic applications over long-haul field fiber links or networks, the engineering of energy–time-entangled photon sources with high compactness, high stability, and high performance is vital.

So far, energy-time entangled photon sources based on continuous-wave (CW) pumped SPDC process have been extensively developed and investigated, either from Type I[17,18] to Type II phase matching[19,20], or from bulk crystal like periodically polarized potassium titanium phosphate (PPKTP)[19,21] to waveguides based on periodically polarized lithium niobate (PPLN)[18,20]. With the merits of the much higher down-conversion efficiency and good mode matching with the optical fibers for photon collection[22], adopting the PPLN waveguide to fabricate a compact energy-time entangled photon pair source is of great interest. Based on a 10 mm-long Type II PPLN waveguide pumped by a 780 nm CW laser, a miniaturized energy-time entangled photon source in telecommunication band has recently been developed[20]. However, as both the pumping of the PPLN and the residual pump filtering in the optical setup involve the structure of free space to fiber coupling, the stability and efficiency of the source, besides the device mass and volume, are far from meeting the requirements for field application.

In this Letter, we report on an upgraded energy-time entangled biphoton source with all-fiber optical configuration. Compared with that reported in Ref. [20], the overall body weight is reduced by 50% to 5 kg with all the physical elements integrated into a cabinet of 36 cm × 21 cm × 16.5 cm for convenience to transport. By monitoring the optical power of the CW laser coupled into the PPLN waveguide, the coupling stability is improved from ±7.6% to ±1.0%; meanwhile, the coupling loss is reduced by 19.1% ± 1.1%. The photon-pair generation efficiency and corresponding purity are investigated as a function of the pump power. At a pump power of 800 μW, the generated photon pairs reach a rate as high as 6.9 MHz with the coincidence to accidental ratio (CAR) better than 1150. By measuring the long-term performances of Hong–Ou–Mandel

(HOM) interference visibility and CAR at a pump power of 60 μW, the stability of the biphoton source has also been tested. Within 10 h of continuous operation, the directly measured HOM visibility without any noise subtracting maintains at 91.8% ± 0.8%, and the CAR is consistently at the level of 10,528.8 ± 604.2. Benefiting from the advantages of compact and lightweight designs, simple production, and high stability, this device provides a reliable biphoton resource for field turn-key quantum communication and metrology applications.

2. Experiment

The sketch of the optical setup and corresponding electrical modules inside the energy-time entangled biphoton source is shown in Fig. 1(a). A distributed Bragg reflector (DBR) fiber-pigtailed single-frequency laser diode (Thorlabs, DBR-780PN) with a typical linewidth of 1 MHz is used as the pump. As the output wavelengths of the DBR laser diode are current- and temperature-tunable, tuning coefficients of the utilized one were measured to be 0.0014 nm/mA and 0.059 nm/°C, respectively. In our case, the wavelength of the DBR laser diode was stabilized to 780.6 nm by fixing its working temperature and current to be 25°C and 100 mA, respectively. At these conditions, a measured optical power of 9.6 mW was emitted from the fiber-pigtailed output. Subsequently, a fiber-based variable optical attenuator (VOA, Thorlabs, VOA780PM-APC) was used to adjust the power injected into a 15 mm-long Type II PPLN waveguide (HC Photonics) with a poling period of 8 μm. By controlling the temperature of the PPLN waveguide at 23.3°C for satisfying the optimized phase-matching condition, the wavelength degenerate signal and idler photons are generated at 1561.2 nm with orthogonal polarizations. To eliminate the residual 780 nm pump, a customized filtering module in combination of a fiber wavelength division multiplexer (WDM, demultiplexing between 1520–1580 nm and 760–810 nm with a division ratio of 50 dB) and a bandpass filter (BP, which has the pass band at 1520–1580 nm and rejects the 780 nm pump by an isolation ratio of 30 dB) was connected behind the output of the PPLN waveguide. Afterwards, the signal and idler photons were spatially separated by a fiber polarization beam splitter (FPBS). To avoid the polarization-dependent instability, all the above-mentioned fiber components were polarization-maintaining. Benefiting from the all-fiber structure, the whole system, including the optics and the control electronics, can be easily integrated into a home-designed 36 cm × 21 cm × 16.5 cm enclosure, and the overall weight is reduced by 50% to 5 kg, as illustrated in Fig. 1(b).

To evaluate the improvement of the upgraded all-fiber energy-time entangled biphoton source, the similar setup utilized in Ref. [20] was reassembled in Fig. 1(c) for comparison. The optical power coupled into the PPLN waveguide was monitored with an optical power meter (OPM, Thorlabs, S122C) when the two DBR laser diodes with different package types were set at the same output power of 14 mW. The HOM interference was used to evaluate the consistency of the energy–time entangled source with the setup shown in Fig. 1(d). The signal and idler passed through a motorized optical delay line (MDL) and a manual optical delay line (ODL), respectively. Then they were coupled into a 50/50 beam splitter (BS) and detected by two superconducting nanowire single-photon detectors (SNSPDs), which were connected to a time-correlated

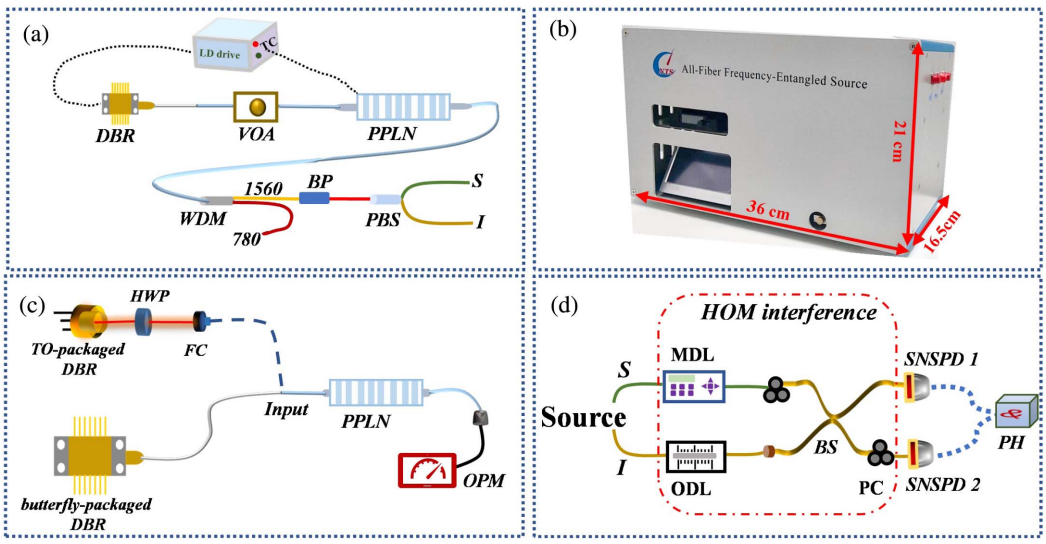

Fig. 1. (a) Components inside the energy-time entangled biphoton source; (b) integrated all-in-one machine and appearance dimensions; (c) setup for monitoring the CW pump laser coupled into the PPLN waveguide; (d) setup for coincidence measurement and evaluating the indistinguishability of the biphotons with HOM interference. DBR, distributed Bragg reflector laser; VOA, variable optical attenuator; PPLN, periodically polarized lithium niobate waveguide; WDM, wavelength division multiplexer; BP, bandpass filter; PBS, polarization beam splitter; HWP, half-wave plate; FC, fiber coupler; OPM, optical power meter; MDL, motorized optical delay line; ODL, manual optical delay line; BS, 50/50 beam splitter; PC, polarization controller; SNSPD, superconducting nanowire single-photon detector; PH, PicoHarp 300.

single-photon counting module (PicoQuant, PicoHarp 300) for coincidence measurement. Two polarization controllers (PCs) were used to adjust the polarization of the propagating photons. In addition, the generated photon pairs were detected by two SNSPDs directly [without the elements in the box of Fig. 1(d)], and the brightness of the photon source was evaluated by recording the coincidence counts and single-photon counts of photons.

3. Results and Discussion

As the coupling power performance from the pump laser to the PPLN waveguide is of great importance for high-efficiency and stable photon pair generation, the optical power of the 780 nm CW pump lasers coupled into the PPLN waveguide was monitored as a quantitative measure. For the transistor outline (TO)-packaged DBR laser diode (Photodigm), an aspherical lens (CFC-2X-B) was used for coupling the free-space beam into the polarization maintaining (PM) fiber pigtail of the waveguide. In addition, a half-wave plate (HWP) at 780 nm was settled before the waveguide to adjust the polarization angle for optimizing the SPDC efficiency. Over the measurement period of 5 h, the output optical power at the PPLN waveguide output was measured as 2.6 ± 0.2 mW, which is shown in Fig. 2 by black dots. When we turned to the butterfly-packaged DBR laser diode with PM pigtail in the all-fiber energy-time entangled biphoton source, the above-mentioned aspherical lens and HWP were no longer necessary, as the PM fibers can be easily coupled and aligned to the polarization axis. Over the same period of measurement, the received optical power after the PPLN waveguide was 5.27 ± 0.05 mW (red triangles in Fig. 2). Compared with our previously developed biphoton source[20], the total coupling and transmission efficiency of the all-fiber pumping scheme were improved from 18.6% to 37.6%, and the power fluctuation was reduced from 7.6% to 1.0%.

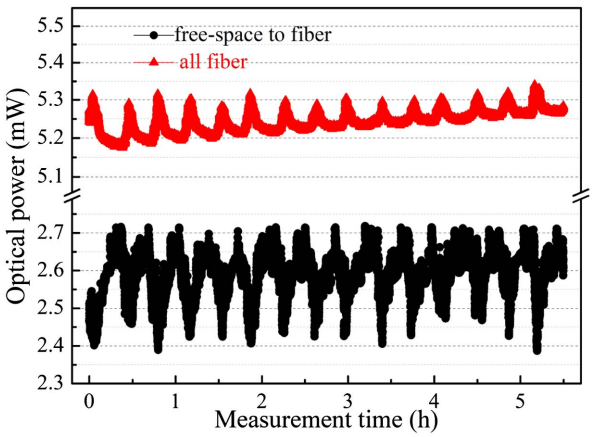

Fig. 2. Comparison of coupled optical power into the PPLN waveguide with two different coupling structures of freespace to fiber (black circles) and all fiber (red triangles).

Figure 3(a) shows the count rates of the signal and the idler photons under different levels of pump power, which can be well fitted linearly except for the region where the detected counts are close to the saturation rate of 1.5 MHz. The inset of Fig. 3(b) indicates a typical coincidence count distribution at the pump power of 150 μW, in which the total coincidence count (C_{tol}) is collected within a time window of 180 ps, which is about 3 times the FWHM of the coincidence count distribution (64 ps), while the accidence coincidence count (A_{cc}) is obtained by averaging the counts within the same time window but 1000 ps away from the coincidence peak. Furthermore, the results of CAR, calculated by $\mathrm{CAR} = (C_{\mathrm{tol}} - A_{\mathrm{cc}})/A_{\mathrm{cc}}$, versus different pump powers are plotted in Fig. 3(b) with orange dots. As expected from theory, the accidental coincidence counts growth is faster than that of the total coincidence counts[23], leading to a degraded CAR with the increase of pump power. At the low pump power, a high CAR up to 80,000 can be observed. When the pump power was increased to 800 μW, the measured CAR dropped to a reasonable level of 1150.

The relations between photon counts in the signal (idler) channel ($N_{s(i)}$), coincidence counts (C_{tol}), and accidental coincidence counts (A_{cc}) can be given by the following expressions[24]:

$$N_{s(i)} = R\eta_{s(i)} + d_{s(i)}, \tag{1}$$

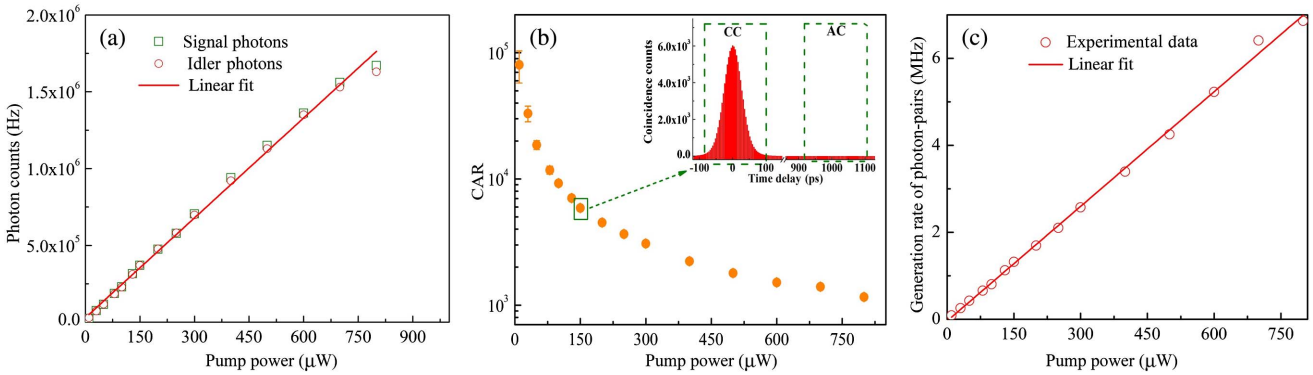

Fig. 3. (a) Detected photon count rates for different pump powers; (b) CAR for different pump powers; inset, typical coincidence counts at a pump power of 150 μW; (c) calculated generation rate of photon pairs for different pump powers.

$$C_{\mathrm{tol}} = R\eta_s\eta_i + A_{\mathrm{cc}}, \tag{2}$$

where R is the generation rate of photon pairs, $\eta_{s(i)}$ is the collection efficiency of the signal (idler) photons, and $d_{s(i)}$ is the dark counting rates of SNSPD in signal (idler) channel. Based on the measured single-photon counting rate, two-photon coincidence count rate, and dark counting rates of the utilized single-photon detection system ($d_{s(i)} \sim 100$), the collection efficiency of the signal (idler) photons was characterized to be ~27.3% and showed weak fluctuation with the change of pump power. Subsequently, the generation rates of photon pairs versus the pump power were calculated and are shown in Fig. 3(c) with the hollow circles, which are linearly fitted by a red solid line with a slope of 8784.90 ± 105.40 Hz/μW, indicating that the generation rate can reach 6.9 MHz at the pump power of 800 μW. Considering the propagation and output coupling efficiency from the PPLN waveguide (η_{WG}~47%), the transmission efficiency of the utilized fiber components (η_F~70%), and the detection efficiency of the SNSPDs ($\eta^d_{s,i} \sim 70\%$), it would give an estimated overall efficiency of $\eta_{s,i} = \eta_{\mathrm{WG}}\eta_F\eta^d_{s,i} \sim 23.0\%$, which is consistent with the above-mentioned photon collection efficiency.

The HOM quantum interference[25] is regarded as an essential tool to evaluate the indistinguishability of the biphotons. When the pump power was set at 60 μW, the HOM interferogram was measured and is shown in Fig. 4(a) with red dots, indicating a visibility $V = 93.6\% \pm 0.47\%$ and an FWHM width of 1.2 ps. It is worth mentioning that the measured HOM interferogram appeared not to have the shape of the standard Mandel dip. Meanwhile, the spectral distributions of the signal and idler photons were identified to have double sidebands around the center wavelength [as shown in Fig. 4(b)], which could be attributed to the fabrication tolerance of the waveguide. Therefore, it is necessary to shape the single-photon spectrum to optimize the HOM interferogram. The modified HOM interferogram after applying a 5 nm fiber-based bandpass filter is also plotted in Fig. 4(a) with black dots, which shows a better-shaped dip but with a broadened temporal width of 2.11 ps due to the narrowing of the spectrum width, while the HOM visibility has no apparent improvement.

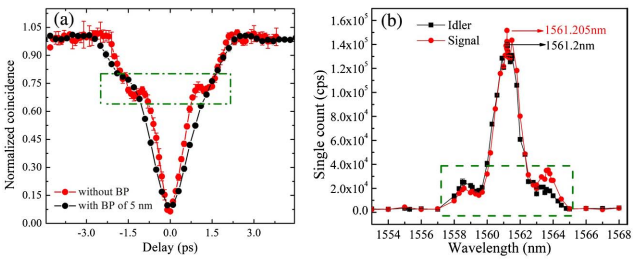

Fig. 4. (a) Measurement of HOM interferograms of unfiltered photons (red dots) and photons with 5 nm BP (black dots); (b) measured single-photon spectral distributions of the signal (red dots) and the idler photons (black dots) that were obtained by scanning the center wavelength of the programmable optical BP (Finisar WaveShaper 4000, 0.08 nm bandwidth) placed in corresponding path, respectively.

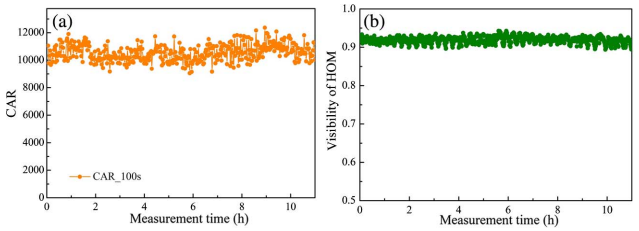

Fig. 5. (a) Long-term stability of CAR and (b) HOM interference visibility in the period of more than 10 h at the pump power of 60 μW.

For field application, the long-term counts and wavelength stability of the energy-time entangled biphoton source is an important criterion. As discussed above, using the all-fiber pumping scheme, the coupling stability between the pump laser and the waveguide was improved significantly. In addition, the stability of the entangled biphoton source is essentially related to the pump wavelength and the phase-matching condition within the SPDC process. As the parameter CAR can visually reflect any wavelength drift of the pump or disturbance in SPDC[26], continuous measurement of the CAR for more than 10 h at a pump power of 60 μW was performed, with results shown in Fig. 5(a). It is seen that, the CAR could maintain the value of 10,528.8 ± 604.2, demonstrating excellent signal-to-noise ratio and stability in the whole measurement period. Note should be taken that the stability of CAR would be further enhanced if the filter with a narrower bandwidth were used. Furthermore, the long-term HOM interference measurement under the same pump power was demonstrated for determining the wavelength stability, as shown in Fig. 5(b). The average visibility of HOM can be sustained at a consistent level of 91.83% ± 0.8%, indicating a good two-photon spectral inseparability.

4. Conclusion

In conclusion, we have presented a significantly upgraded energy-time entangled biphoton source based on the SPDC in a Type II PPLN waveguide with an all-fiber optical configuration, allowing all the physical elements integrated into a compact cabinet. Benefiting from the advantages of all polarization-maintaining fiber optics, the coupling efficiency and stability of the pump laser to the waveguide are significantly improved compared with its predecessor. With the measured single-photon and two-photon coincidence counts, the CAR and generated photon pairs rates are obtained at different pump powers. With a pump power of 800 μW, the generated photon pairs reach a rate of 6.9 MHz, with the CAR better than 1150. Furthermore, the long-term performance of HOM interference visibility and CAR at a pump power of 60 μW have also been tested. Within 10 h of continuous operation, the directly measured HOM visibility without any noise subtracting maintains at 91.8% ± 0.8%, and the CAR is consistently at the level of 10, 528.8 ± 604.2. This portable device provides a reliable and

efficient biphoton source for field turnkey quantum communication and metrology applications.

Acknowledgement

This work was supported by the National Natural Science Foundation of China (Nos. 12033007, 61875205, 91836301, 12103058, and 61801458), the Western Young Scholar Project of CAS (Nos. XAB2019B17 and XAB2019B15), the Frontier Science Key Research Project of CAS (No. QYZDB-SSW-SLH007), the Strategic Priority Research Program of CAS (No. XDC07020200), and the Youth Innovation Promotion Association, CAS (Nos. 2022413 and 2021408).

References

1. H. J. Kimble, "The quantum internet," Nature **453**, 1023 (2008).
2. J. D. Franson, "Nonlocal cancellation of dispersion," Phys. Rev. A **45**, 3126 (1992).
3. R. Quan, Y. Zhai, M. Wang, F. Hou, S. Wang, X. Xiang, T. Liu, S. Zhang, and R. Dong, "Demonstration of quantum synchronization based on second-order quantum coherence of entangled photons," Sci. Rep. **6**, 30453 (2016).
4. F. Hou, R. Quan, R. Dong, X. Xiang, B. Li, T. Liu, X. Yang, H. Li, L. You, Z. Wang, and S. Zhang, "Fiber-optic two-way quantum time transfer with frequency-entangled pulses," Phys. Rev. A. **100**, 023849 (2019).
5. R. Quan, R. Dong, Y. Zhai, F. Hou, X. Xiang, H. Zhou, C. Lv, Z. Wang, L. You, T. Liu, and S. Zhang, "Simulation and realization of a second-order quantum-interference-based quantum clock synchronization at the femtosecond level," Opt. Lett. **44**, 614 (2019).
6. Y. Liu, R. Quan, X. Xiang, H. Hong, M. Cao, T. Liu, R. Dong, and S. Zhang, "Quantum clock synchronization over 20-km multiple segmented fibers with frequency-correlated photon pairs and HOM interference," Appl. Phys. Lett. **119**, 144003 (2021).
7. M. Xie, H. Zhang, Z. Lin, and G. L. Long, "Implementation of a twin-beam state-based clock synchronization system with dispersion-free HOM feedback," Opt. Express **29**, 28607 (2021).
8. H. Hong, R. Quan, X. Xiang, W. Xue, H. Quan, W. Zhao, Y. Liu, M. Cao, T. Liu, S. Zhang, and R. Dong, "Demonstration of 50 km fiber-optic two-way quantum clock synchronization," J. Light. Technol. **40**, 3723 (2022).
9. R. Quan, H. Hong, W. Xue, H. Quan, W. Zhao, X. Xiang, Y. Liu, M. Cao, T. Liu, S. Zhang, and R. Dong, "Implementation of field two-way quantum synchronization of distant clocks across a 7 km deployed fiber link," Opt. Express **30**, 10269 (2022).
10. J. Nunn, L. J. Wright, C. Sller, L. Zhang, and B. J. Smith, "Large-alphabet time-frequency entangled quantum key distribution by means of time-to-frequency conversion," Opt. Express **21**, 15959 (2013).
11. M. Y. Niu, F. Xu, J. H. Shapiro, and F. Furrer, "Finite-key analysis for time-energy high-dimensional quantum key distribution," Phys. Rev. A **94**, 52323 (2016).
12. S. P. Neumann, D. Ribezzo, M. Bohmann, and R. Ursin, "Experimentally optimizing QKD rates via nonlocal dispersion compensation," Quantum Sci. Technol. **6**, 025017 (2021).
13. Y. Xue, W. Chen, S. Wang, Z. Yin, L. Shi, and Z. Han, "Airborne quantum key distribution: a review [Invited]," Chin. Opt. Lett. **19**, 122702 (2021).
14. B. Li, F. Hou, R. Quan, R. Dong, L. You, H. Li, X. Xiang, T. Liu, and S. Zhang, "Nonlocality test of energy-time entanglement via nonlocal dispersion cancellation with nonlocal detection," Phys. Rev. A **100**, 053803 (2019).
15. X. Xiang, R. Dong, B. Li, F. Hou, R. Quan, T. Liu, and S. Zhang, "Quantification of nonlocal dispersion cancellation for finite frequency entanglement," Opt. Express **28**, 17697 (2020).
16. Y. Jin, Y. Yang, H. Hong, X. Xiang, R. Quan, T. Liu, S. Zhang, N. Zhu, M. Li, and R. Dong, "Quantum microwave photonics in radio-over-fiber systems," Photonics Res. **10**, 1669 (2022).
17. R. Horn, P. Abolghasem, B. J. Bijlani, D. Kang, A. S. Helmy, and G. Weihs, "Monolithic source of photon pairs," Phys. Rev. Lett. **108**, 153605 (2012).
18. P. Lefebvre, R. Valivarthi, Q. Zhou, L. Oesterling, D. Oblak, and W. Tittel, "Compact energy–time entanglement source using cascaded nonlinear interactions," J. Opt. Soc. Am. B **38**, 1380 (2021).
19. F. Hou, X. Xiang, R. Quan, M. Wang, Y. Zhai, S. Wang, T. Liu, S. Zhang, and R. Dong, "An efficient source of frequency anti-correlated entanglement at telecom wavelength," Appl. Phys. B **122**, 128 (2016).
20. Y. Zhang, F. Hou, T. Liu, X. Zhang, S. Zhang, and R. Dong, "Generation and quantum characterization of miniaturized frequency entangled source in telecommunication band based on type-II periodically poled lithium niobate waveguide," Acta Phys. Sin. **67**, 144204 (2018).
21. S. Ramelow, L. Ratschbacher, A. Fedrizzi, N. K. Langford, and A. Zeilinger, "Discrete tunable color entanglement," Phys. Rev. Lett. **103**, 253601 (2009).
22. S. Tanzilli, W. Tittel, H. De Riedmatten, H. Zbinden, P. Baldi, M. DeMicheli, D. B. Ostrowsky, and N. Gisin, "PPLN waveguide for quantum communication," Eur. Phys. J. D **18**, 155 (2002).
23. M. Bock, A. Lenhard, C. Chunnilall, and C. Becher, "Highly efficient heralded single-photon source for telecom wavelengths based on a PPLN waveguide," Opt. Express **24**, 23992 (2016).
24. Z. Zhang, C. Yuan, S. Shen, H. Yu, R. Zhang, H. Wang, H. Li, Y. Wang, G. Deng, Z. Wang, L. You, Z. Wang, H. Song, G. Guo, and Q. Zhou, "High-performance quantum entanglement generation via cascaded second-order nonlinear processes," NPJ Quantum Inf. **7**, 123 (2021).
25. C. K. Hong, Z. Y. Ou, and L. Mandel, "Measurement of subpicosecond time intervals between two photons by interference," Phys. Rev. Lett. **59**, 2044 (1987).
26. C. Chen, A. Riazi, E. Y. Zhu, M. Ng, A. V. Gladyshev, and P. G. Kazansky, "Turn-key diode-pumped all-fiber broadband polarization-entangled photon source," OSA Contin. **1**, 981 (2018).